Macromolecules

Article

Cite This: Macromolecules 2018, 51, 1529−1538

Effects of Chain Topology on the Self-Assembly of AB-Type Block Copolymers

Wenbo Jiang,[†,¶] Yicheng Qiang,[†,¶] Weihua Li,[*,†] Feng Qiu,[†] and An-Chang Shi[‡]

[†]State Key Laboratory of Molecular Engineering of Polymers, Key Laboratory of Computational Physical Sciences, Department of Macromolecular Science, Fudan University, Shanghai 200433, China

[‡]Department of Physics and Astronomy, McMaster University, Hamilton, Ontario L8S 4M1, Canada

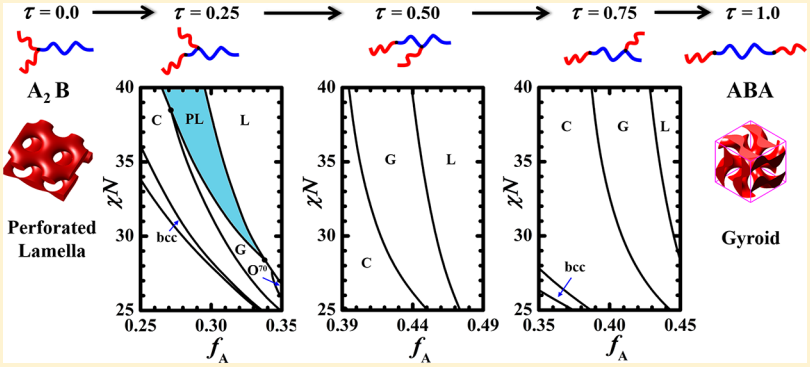

ABSTRACT: The effects of chain topology on the self-assembly of block copolymers are examined using an ABA_T block copolymer, composed of an AB diblock copolymer with an extra A block tethered onto the B block, as a model system. The topology of the ABA_T block copolymer is regulated by the tethering point, such that the block copolymer changes continuously from linear ABA triblock copolymer to A_2B miktoarm star copolymer as the tethering position moves from the B end to the AB junction. The phase diagrams of ABA_T copolymers of different tethering positions are constructed using the self-consistent field theory. The theoretical results reveal that the phase behavior of the system depends sensitively on the topology of the ABA_T copolymers. In particular, a considerably wide stable region of the perforated lamellar (PL) phase is predicted for ABA_T with proper tethering positions. The PL phase could even completely replaces the gyroid phase at relatively strong segregation. Furthermore, a large window of the hexagonally close-packed (hcp) spherical phase, as well as a direct transition from hcp to the cylindrical phase, is predicted. An analysis of the distributions of the different blocks reveals that the local segregation of the two different B blocks occurs to accommodate the topological constraints due to the chain architecture, which in turn regulates the local interfacial curvature and chain packing resulting in the different phase behaviors.

INTRODUCTION

The self-assembly of block copolymers continues to attract tremendous attention due to its unique ability to form rich ordered nanostructures.[1−4] In particular, the linear AB diblock copolymer composed of A and B subchains tethered at their ends has been intensively studied by experiment and theory.[5−12] It has been established that the phase behavior of the AB diblock copolymer is mainly governed by two controlling parameters, the volume fraction f of the A blocks and the interaction parameter χN where N is the total polymerization index and χ is the Flory−Huggins parameter characterizing the immiscibility of the two dissimilar monomers. A relatively complete phase diagram of AB diblock has been constructed through the concerted interplay between experiment and theory over the past few decades.[10] It was believed that AB diblock copolymers could form a number of ordered phases including hexagonally close packed (hcp) spheres, body-centered cubic (bcc) spheres, hexagonally packed cylinders (C), lamellae (L), double gyroid (G), and *Fddd* (O^{70}) bicontinuous networks.[5,7,11−14] Recently, a number of complex spherical packing phases have been observed in AB diblock copolymers (e.g., PI-*b*-PLA) by experiment.[15−17] The stability of the complex spherical packing phases, in particular the Frank−Kasper σ phase, has been examined using the self-consistent field theory (SCFT).[18,19] These studies revealed that the σ phase could be stabilized by the conformational asymmetry between the A and B blocks.

It is well-known that chain architecture of block copolymers provides another parameter controlling their self-assembly behaviors. With the development of modern synthesis techniques,[20,21] block copolymers with different architectures become accessible.[3,22−26] For the simplest case of two types of monomers, or AB-type copolymers, the architecture of the copolymer chain could be varied as a function of the number of

Received: November 10, 2017
Revised: February 13, 2018
Published: February 15, 2018

DOI: 10.1021/acs.macromol.7b02389
Macromolecules 2018, 51, 1529−1538

repeating blocks and the chain topology. A large number of AB-type block copolymers with different architectures, such as linear ABA triblock,[27−32] AB_n miktoarm star,[18,33−36] $(AB)_n$ star,[24,37−39] comb,[25,40,41] ABAB⋯,[22,42−46] and $(BAB)_n$ star,[47,48] have been studied by both experiment and theory. A general observation from the previous studies is that the phase behavior of many of these different AB-type block copolymers resembles that of an AB diblock copolymer except the phase boundaries of the various order-to-order transitions are shifted. However, it has also revealed that some of these copolymers could form nonclassical ordered phases. For example, a narrow channel of the perforated lamellar (PL) phase is predicted in AB_n (or equivalently A_nB) and AB comb copolymers.[14] Moreover, stable Frank−Kasper σ and A15 phases are also observed in AB_n copolymers as a result of the enhanced conformational asymmetry by the branching architecture.[18,35] Another interesting example is that a square array of cylinders could be stabilized by the effect of combinatorial entropy arising from the maximization of configurations of multiarm star copolymers.[48−50]

One interesting effect of chain topology is the different phase behaviors of the linear ABA triblock copolymers and A_2B miktoarm star copolymers. Specifically, previous SCFT studies have predicted that the PL and σ phases are stable phases of A_2B star copolymers, whereas they are metastable phases of linear ABA triblock copolymers.[14,18] It should be noted that the A_2B and ABA copolymers have the same number of blocks but different topology, and these two copolymers could be obtained by grafting an additional A block onto the B block of an AB diblock copolymer at the junction point and at the end of the B block, respectively. The different phase behaviors of these two copolymers imply that the topology of the block copolymers must have a significant impact on the self-assemblies of the systems.

Among the different ordered phases of diblock copolymers, the PL phase presents an interesting case due to its unique morphology. The PL phase is a variation of the familiar lamellar phase, in which an array of pores are formed in the minority layers. Earlier experiments suggested that the PL phase could be one equilibrium phase of diblock copolymers,[5,8] but later experimental and theoretical studies have confirmed that the PL phase is a metastable phase of diblock copolymers.[10] It is well-known that the PL phase is usually less stable than the double gyroid phase in many AB type block copolymers. The origin of this observation is that, compared with the gyroid phase, the PL structure composed of lamellae with pores has a lower mean interfacial curvature but with a much larger curvature variation.[10] In order to stabilize the PL morphology, it is critical to reduce the energy penalty associated with the highly nonuniform distribution of the interfacial curvature. Besides varying the chain architecture to be nonlinear, e.g., branched or comb-like, another useful method is using polymer blends. For example, adding A homopolymers to AB diblock copolymers could stabilize the PL morphology with perforated B layer.[51,52] However, to the best of our knowledge, only a very narrow stable region of the PL phase is predicted with various block copolymer systems by theory,[14,51,52] although the PL morphologies have been observed with PI-*b*-PS diblock[8] and asymmetric PS-*b*-PB-*b*-PS triblock[32] copolymers in experiments.

Inspired by the different phase behaviors of the miktoarm A_2B and linear ABA triblock copolymers, we designed a model block copolymer by varying the tethering point of the second A block along the B block, resulting in a series of AB-type block copolymers (schematic shown in Figure 1a). These ABA_T block copolymers, where the subscript "T" indicates the tethering of the additional A block onto the B block, provide a model system to examine the effects of chain topology on the self-assembly of block copolymers, as well as to obtain stable PL phase with a larger stability region for potential applications. The fundamental idea is to stabilize the PL phase with perforated A layer by using the tethering position to regulate the distribution of the two different B blocks to accommodate to the A/B interfaces with different curvatures. In other words, different spontaneous curvatures could be generated via the two B blocks by regulating their topological environment. For the PL structure, the curvature variation of the A/B interfaces mainly originates from the two very different areas, i.e. the layers and the pores. If the two B blocks could be preferentially distributed to the two areas, the energy penalty caused by the highly nonuniform curvature could be reduced, thus stabilizing the PL phase. We will verify the validity of this designing idea by constructing the phase diagrams of ABA_T copolymers with various tethering positions using SCFT.

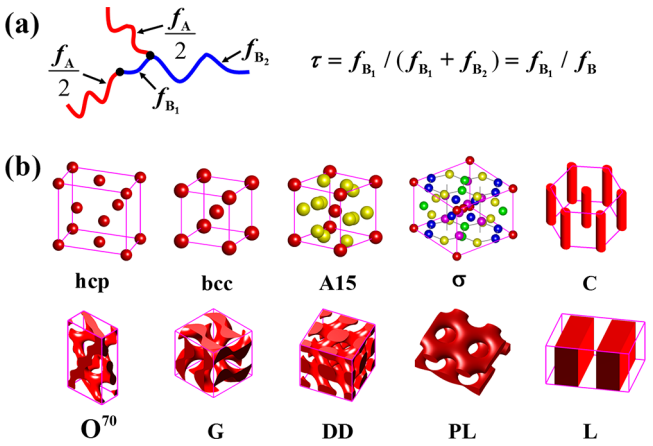

Figure 1. (a) Schematic of ABA_T block copolymer composed of AB diblock with an additional A block tethered onto the B block. The B block is subdivided by the tethering point into B_1 and B_2 blocks. The tethering position is characterized by $\tau = f_{B_1}/(f_{B_1} + f_{B_2}) = f_{B_1}/f_B$. $\tau = 0$ and $\tau = 1$ indicate A_2B miktoarm star and ABA triblock copolymers, respectively. (b) Schematics of the candidate ordered phases considered in the current study.

THEORY AND METHOD

The SCFT is a flexible and powerful theoretical framework for the study of inhomogeneous polymer systems. It has become a standard tool, similar to some of the experimental techniques, such as transmission electron microscope (TEM) and small-angle X-ray scattering (SAXS), for the study of the phase behavior of polymeric systems. In particular, for flexible polymers modeled as ideal Gaussian chains, the SCFT provides an efficient and accurate framework to calculate the free energy of different ordered phases.[10,53] Moreover, the SCFT is capable to treat any architecture of polymers readily from linear,[27,42,54,55] to branched,[18,35] or even superbranched.[56,57] As a result of these development, the SCFT has been widely used to study the phase behavior of flexible block copolymers and the SCFT predictions are in good agreement with experimental observations.[10]

DOI: 10.1021/acs.macromol.7b02389
Macromolecules 2018, 51, 1529−1538

Detailed formulation and derivation of SCFT will not be given here because they are readily found in the literature.[7,58,59] For the convenience of discussions, we will list expressions for the free-energy functional and the standard SCFT equations below. For an AB-type block copolymer melts contained in a volume V at temperature T, its free energy per chain in the unit of thermal energy k_BT, where k_B is the Boltzmann constant, is given by

$$\frac{F}{nk_BT} = -\ln Q + \frac{1}{V}\int d\mathbf{r}\,\{\chi N\phi_A(\mathbf{r})\phi_B(\mathbf{r}) - w_A(\mathbf{r})\phi_A(\mathbf{r}) - w_B(\mathbf{r})\phi_B(\mathbf{r}) - \eta(\mathbf{r})[1 - \phi_A(\mathbf{r}) - \phi_B(\mathbf{r})]\} \quad (1)$$

In this expression of the free energy, $\phi_A(\mathbf{r})$ and $\phi_B(\mathbf{r})$ are the volume fraction distributions of A and B, while $w_A(\mathbf{r})$ and $w_B(\mathbf{r})$ are their conjugate mean fields, respectively. The function $\eta(\mathbf{r})$ is a Lagrange multiplier used to enforce the incompressibility condition, $\phi_A(\mathbf{r}) + \phi_B(\mathbf{r}) = 1$. The constant Q is the partition function of a single block copolymer interacting with the mean fields $w_A(\mathbf{r})$ and $w_B(\mathbf{r})$.

For an incompressible polymer melt, the number of polymer chains, n, contained in the volume is proportional to V, e.g., $n = V\rho_0/N$ where ρ_0 and N are the segment density and number of segments or degree of polymerization of the polymers, respectively. For the model AB-type copolymers (ABA_T) considered in the current work, the total number of A and B segments is specified by f_AN and f_BN, respectively. We will choose to divide the A segments equally between the two A blocks (Figure 1a), such that the segment number of each A block is $f_AN/2$. Additionally, the segment number of the middle and tail B blocks is specified as $f_{B_1}N$ and $f_{B_2}N$, respectively. A parameter, $\tau = f_{B_1}/f_B$, is introduced to characterize the tethering position of the ABA_T copolymers. The parameter τ is defined to specify the topology of the ABA_T such that it becomes the A_2B at $\tau = 0$ and ABA at $\tau = 1$, respectively.

The SCFT equations associated with the free energy functional given by eq 1 are written as[59]

$$w_A(\mathbf{r}) = \chi N\phi_B(\mathbf{r}) + \eta(\mathbf{r}) \quad (2)$$

$$w_B(\mathbf{r}) = \chi N\phi_A(\mathbf{r}) + \eta(\mathbf{r}) \quad (3)$$

$$\phi_A(\mathbf{r}) = \frac{1}{Q}\int_{s\in A} ds\; q(\mathbf{r}, s)q^{\dagger}(\mathbf{r}, s) \quad (4)$$

$$\phi_B(\mathbf{r}) = \frac{1}{Q}\int_{s\in B} ds\; q(\mathbf{r}, s)q^{\dagger}(\mathbf{r}, s) \quad (5)$$

$$Q = \frac{1}{V}\int d\mathbf{r}\; q(\mathbf{r}, s)q^{\dagger}(\mathbf{r}, s) \quad (6)$$

Here $q(\mathbf{r}, s)$ and $q^{\dagger}(\mathbf{r}, s)$ are the propagators of the polymer chain. These propagators satisfy the following modified diffusion equations,

$$\frac{\partial q(\mathbf{r}, s)}{\partial s} = \nabla^2 q(\mathbf{r}, s) - w(\mathbf{r}, s)q(\mathbf{r}, s) \quad (7)$$

$$-\frac{\partial q^{\dagger}(\mathbf{r}, s)}{\partial s} = \nabla^2 q^{\dagger}(\mathbf{r}, s) - w(\mathbf{r}, s)q^{\dagger}(\mathbf{r}, s) \quad (8)$$

where $w(\mathbf{r}, s) = w_K(\mathbf{r})$ when s belongs to the K blocks (K = A and B). In the above expressions, the radius of gyration of an unperturbed homopolymer chain with N segments, $R_g = N^{1/2}b/\sqrt{6}$ is chosen as the unit of length.

The SCFT equations form a set of nonlinear and nonlocal equations, which need to be solved numerically to obtain solutions corresponding to different ordered phases. In recent decades, a number of numerical schemes have been developed to solve the SCFT equations.[60−62] In the current study we implement the pseudospectral method[60,61] coupled with the Anderson mixing iteration scheme[62] to solve the SCFT equations, the efficiency of which has been demonstrated in various block copolymer systems.[63] Furthermore, we have included a large number of ordered morphologies (shown in Figure 1b) as the candidate phases in the study. Specifically, numerical solutions of the SCFT equations corresponding to these candidates were obtained. The phase diagram of the system is then constructed by a comparison of the free energy of these phases.

In order to obtain reliable accuracy with the phase boundaries, the unit box is discretized into a $N_x \times N_y \times N_z$ grid lattice with $N_x \times N_y \times N_z = 128 \times 128 \times 64$ for the Frank−Kasper σ phase with a large unit cell while $N_x \times N_y \times N_z = 64^3$ for the other ordered phases. Of course, for the cylindrical or lamellar phase with translational symmetry along one or two dimensions, the computational dimensions are reduced accordingly. With such grid lattices, the three grid spacings are ensured to be smaller than $0.15R_g$. Additionally, the chain contour is divided into $N_s = 200$ or 400 points. Similar to our previous work,[64] we have checked that the influence of the calculation errors on the accuracy of the phase boundaries can be safely ignored.

Note that the free energy is minimized with respect to the box sizes. The optimization process for the ordered phases with only one period (e.g., hcp, bcc, G, *Fddd*, C, and L phases) is much faster than that for those ordered phases with two periods (e.g., the Frank−Kasper σ and PL phases). In our calculations, 3−6 points are needed to optimize the period of each one-period phase, while 10−20 points for each two-period phase because its two periods are optimized alternatively in cycles. Therefore, the calculation labor for the construction of a two-dimensional phase diagram typically consisting of more than 100 transition points is quite heavy, especially with the portion involving the full three-dimensional ordered phases with two periods (σ and PL). For example, one run of free-energy calculation on a CPU of Intel Xeon Processor E5−2690 V4 2.6 GHz takes about 1.5h for $N_s = 200$ and $N_x \times N_y \times N_z = 64^3$ while 8h for $N_s = 200$ and $N_x \times N_y \times N_z = 128 \times 128 \times 64$. Excluding a lot of extra time used to screen out the candidate phases for each phase boundary, we roughly estimate the total calculation time for a typical phase diagram as 5000 CPU hours, which is affordable for modern computational facilities.

RESULTS AND DISCUSSION

Phase Diagrams. To examine the effect of the tethering position on the phase behavior of ABA_T copolymers, we first present three phase diagrams for three typical tethering positions at $\tau = 0.25$, 0.5, and 0.75 (Figure 2). The completeness of the phase diagram relies critically on the library of candidate phases. In order to make the structure library as complete as possible, we included ten ordered phases (Figure 1b) in our calculations. The classical spherical phases of hexagonally close-packed (hcp) and body-centered cubic (bcc), the two network phases of double gyroid (G) and *Fddd* (O^{70}), the hexagonal phase of cylinders (C) and the lamellar phase

DOI: 10.1021/acs.macromol.7b02389
Macromolecules 2018, 51, 1529−1538

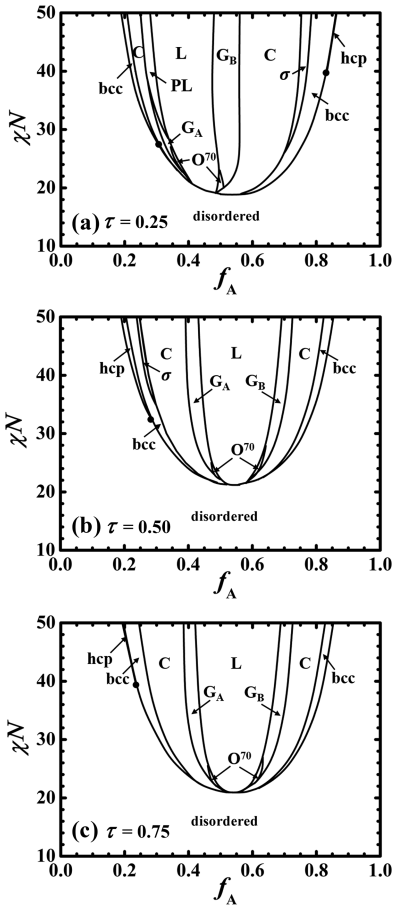

Figure 2. Phase diagrams of ABA_T copolymers with respect to f_A and χN for three different tethering positions: (a) $\tau = 0.25$, (b) $\tau = 0.5$, and (c) $\tau = 0.75$.

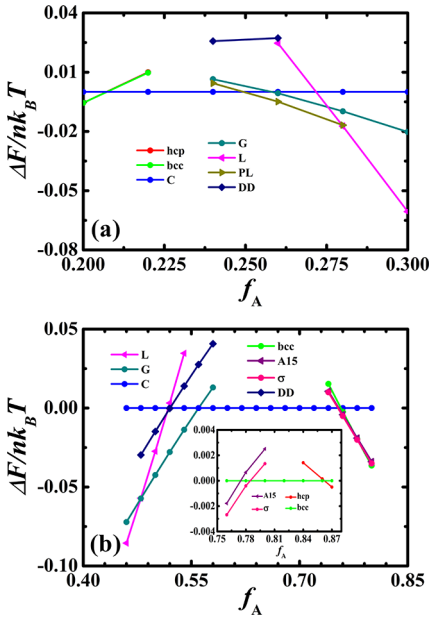

Figure 3. Free energies of considered ordered phases relative to that of the cylinder phase (C) for $\tau = 0.25$ and $\chi N = 50$: (a) $0.2 \leq f_A \leq 0.3$ going through the sequence of ordered phases of bcc → C→PL → L; (b) $0.46 \leq f_A \leq 0.8$ going through the inverse sequence of L → G → C → σ → bcc → hcp. For the reason for clarity, the inset in part b shows the free energies of spherical packing phases relative to that of bcc.

(L) are commonly observed in AB-type block copolymers.[11−14,27,42] The two nonclassical spherical packing phases, the Frank−Kasper σ and A15, are predicted to be equilibrium phases of A_2B ($\tau = 0$) block copolymers.[18,56] Moreover, the double diamond (DD) phase is always an interesting competing network phase with G and PL.[10]

An obvious and nontrivial result is that the phase behaviors of ABA_T depends on the tethering position, as the macromolecule changes from A_2B-like to ABA-like as τ is changed from 0 to 1. It is further observed that interesting phase behavior occurs for intermediate values of τ, *e.g.* $\tau = 0.25$. One of the most remarkable features in the phase diagram shown in Figure 2a is that the PL phase exhibits a considerable stability region that completely replaces the gyroid phase at the relatively strong segregation of $\chi N \gtrsim 38.45$. This unexpected behavior is clearly shown in the free energy plot of the different ordered phases for $\chi N = 50$ shown in Figure 3. The two triple points (C/PL/G and G/PL/L) are located at $(f_A, \chi N) \approx (0.272, 38.45)$ and $(0.336, 28.50)$, respectively. In contrast to A_2B, the stable region of PL widens drastically, e.g. that it increases from $\Delta f_{PL} \approx 0.006$ in A_2B to $\Delta f_{PL} \approx 0.030$ for $\tau = 0.25$ and $\chi N = 50$. In addition, the stability region of the conjugate gyroid phase G_B with B-domain networks is also noticeably widened from $\Delta f_{G_B} \approx 0.035$ in A_2B to $\Delta f_{G_B} \approx 0.080$ for $\chi N = 50$. It is noted that $\Delta f_{G_B} \approx 0.080$ in the phase diagram of $\tau = 0.25$ is also considerably larger than $\Delta f_{G_B} \approx 0.025$ in AB diblock or ABA triblock copolymers for $\chi N = 50$.[14] As a result, the enlarged phase region of G_B expands beyond $f_A = 0.5$ toward the left side of the phase diagram.

Another interesting feature of the phase diagram with $\tau = 0.25$ is the shrinking region of the σ phase, which could be attributed to the reduced conformational asymmetry. Intuitively, the conformation between the A and B blocks changes continuously from the most asymmetric in A_2B to the most symmetric in ABA. As a consequence, the asymmetry of the phase diagrams tapers off as τ increases. However, it is very surprising that a noticeable stability region of σ is observed in the left side of the phase diagram with $\tau = 0.5$ in Figure 2b. The switch of the σ region from the right side ($f_A > 0.5$) to the left side ($f_A < 0.5$) of the phase diagrams implies a switch of the conformational asymmetry between the A and B blocks. In contrast, the phase diagram of $\tau = 0.75$ shown in Figure 2c shows less pronounced features as it is simply similar to that of ABA, indicating that the short tail of B_2 block does not have a significant influence on the phase behaviors of the system.

The obvious contrast between the three phase diagrams in Figure 2 clearly demonstrates the nontrivial effect of the tethering position of the second A block onto the B block. To demonstrate this effect more explicitly, we construct a phase diagram with respect to τ and f_A for a fixed $\chi N = 50$ shown in Figure 4. This phase diagram shows that the stable region of PL gradually widens and reaches the largest width at $\tau \approx 0.24$, and then tapers off until vanishing at $\tau \approx 0.29$. For $\tau < 0.23$, the expansion of the PL-region is accompanied by the shrinking of that of G-region, and the total region of the two phases does not change observably. Interestingly, the phase region of G terminates at $\tau \approx 0.23$ and reappears when the PL-region vanishes at $\tau \approx 0.29$. This observation is consistent with the results from the phase diagrams shown in Figure 2, where the whole phase region of G in Figure 2a with $\tau = 0.25$ is replaced

DOI: 10.1021/acs.macromol.7b02389
Macromolecules 2018, 51, 1529−1538

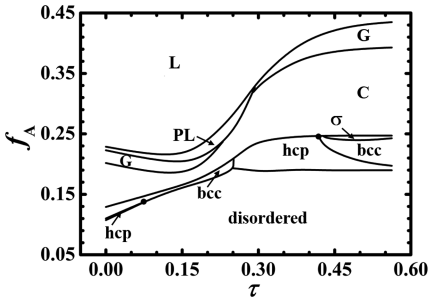

Figure 4. Phase diagrams of ABA_T copolymers with respect to τ and f_A for $\chi N = 50$.

by that of PL when $\chi N > 38.45$ while no stable PL is observed in Figure 2b with $\tau = 0.5$.

It is well-known that the hcp spherical phase usually occupies a very narrow stability channel at the vicinity of order−disorder transition (ODT) for many AB-type block copolymers, i.e. intermediate between the disordered (D) phase and the bcc spherical phase.[14] Surprisingly, the stability of hcp relative to bcc is sensitively dependent on the tethering position or the chain topology in the current model system. As the tethering position moves from the AB junction point to the B end, the narrow hcp-region vanishes at a triple point of $(\tau, f_A) \approx (0.07, 0.135)$. In other words, the disordered phase would directly transfer to the bcc phase without going through the hcp phase in the region of $0.07 < \tau < 0.25$. At $\tau \gtrsim 0.25$, the phase region of bcc suddenly terminates and is replaced by a wider region of hcp. The largest width of the phase region of hcp reaches $\Delta f_A \approx 0.054$, which is 6−27 times of that in A_2B miktoarm, ABA triblock, or AB diblock copolymers. This unusual wide region of hcp is evidenced by the free energy comparison at $\tau = 0.375$ in Figure 5. It is expected that such a large window of the hcp

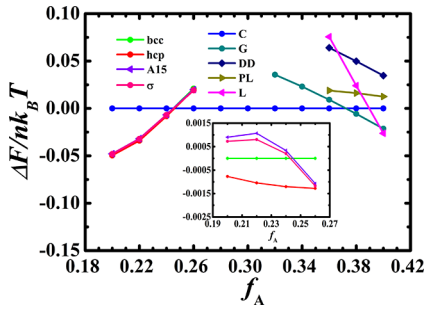

Figure 5. Free energy comparison of considered ordered phases relative to that of the cylinder phase (C) along the typical phase path of $\tau = {}^3/_8$ in Figure 4, indicating a large window of the hcp spherical phase. For the reason for clarity, the inset shows the free energies of considered spherical phases relative to that of bcc.

phase in the parameter space would facilitate its observation in experiments. Note that we do not extend the phase diagram to $\tau > 0.6$ because the phase behavior of the ABA_T copolymer tends to approach that of ABA as τ increases.

Mechanisms Stabilizing Nonclassical Phases. The above SCFT results demonstrate that adjusting the tethering position of the ABA_T block copolymer provides a useful route to regulate the relative stability between the PL and G phases as well as that between the hcp and bcc phases. In the following, we turn to probing into the stabilization mechanism of PL and hcp relative to G and bcc. One of the advantages of the SCFT is that the solutions could be used to obtain various contributions of free energy including the interfacial and entropic contributions,[10] which enables us to reveal how each contribution is influenced by the change of the tethering position. In addition, SCFT can generate the distribution of each segment, which is also a good breakthrough point for exploring the stabilization mechanism of considered phases.

Intuitively, the PL phase should be unfavorable entropically when compared with the G phase because of the existence of the pores resulting in large variations in the interfacial curvature. To confirm this speculation, we compare the interfacial free energy $[U/nk_BT = 1/V\int d\mathbf{r}\ \chi N\phi_A(\mathbf{r})\phi_B(\mathbf{r})]$ and entropic contribution to the free energy $\{-TS/nk_BT = -\ln Q - 1/V\int d\mathbf{r}\ [w_A(\mathbf{r})\phi_A(\mathbf{r}) + w_B(\mathbf{r})\ \phi_B(\mathbf{r})]\}$ of the PL phase with those of the G phase for a fixed value of $\chi N = 50$ in Figure 6.[10] Three typical tethering positions, $\tau = 0$ (e.g., A_2B), $\tau =$

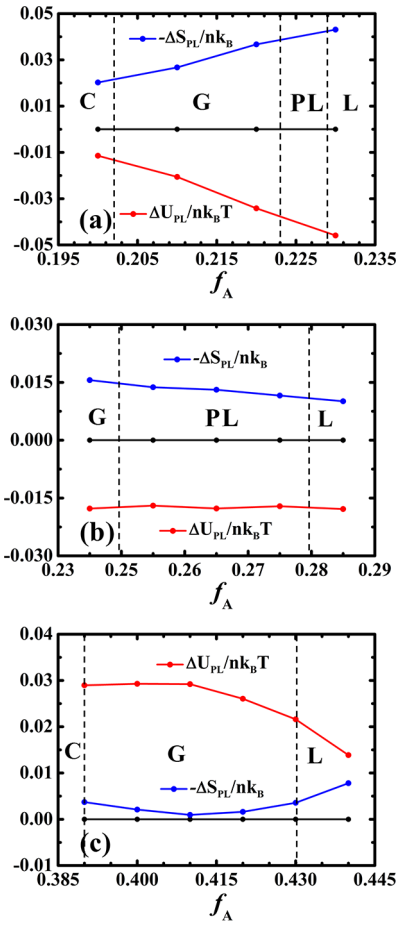

Figure 6. Interfacial and entropic contributions to the free energy of the PL phase relative to the gyroid phase, $\Delta U/nk_BT$ and $-\Delta S/nk_B$, at $\chi N = 50$ for three different values: (a) $\tau = 0$ (e.g., A_2B), (b) $\tau = 0.25$, and (c) $\tau = 0.5$. The dashed lines in parts a−c indicate the phase boundaries.

0.25, and $\tau = 0.5$, are considered in Figure 6, leading to three behaviors for the PL phase. In the case of $\tau = 0.25$ (Figure 6b) the PL phase completely replaces the gyroid phase. In the case of $\tau = 0$ (Figure 6a), the PL phase only occupies a narrow window in the phase diagram. On the other hand, the PL is not a stable phase in the case of $\tau = 0.5$ (Figure 6c). As expected, the entropic contribution to the free energy for the PL phase is always higher than that of G in the three cases. This

DOI: 10.1021/acs.macromol.7b02389
Macromolecules 2018, 51, 1529−1538

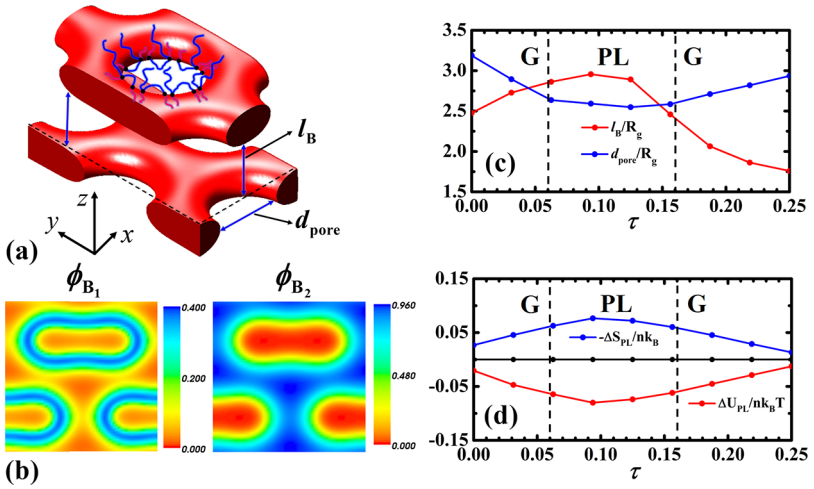

Figure 7. (a) Schematics for the typical configurations of the ABA_T copolymers around the pore in the isosurface plot of the PL morphology, where d_{pore} and l_B indicate the diameter of the pore and the thickness of B layer or the interval between two neighboring A layers, respectively. (b) Two dimensional density distributions of B_1 and B_2 blocks in the cross-section of the stable PL morphology going through the center of the pore at the yz plane for χN = 50, f_A = 0.26, and τ = 0.25, where A and B are indicated by red and blue colors, respectively. (c) Variation of d_{pore} and l_B along the typical phase path of f_A = 0.21 in Figure 4. (d) the corresponding interfacial and entropic contributions of PL relative to G, $\Delta U/nk_BT$, and $-\Delta S/nk_B$, for the same phase path in part c.

observation reveals that the PL phase is mainly stabilized by regulating the interfacial free energy with the tethering position. In Figure 6b, the interfacial free energy of the PL phase is consistently lower than that of G. This reduction of the interfacial free energy is enough to compensates the entropic penalty due to its more nonuniform curvature, thus stabilizing the PL phase relative to the G phase. In contrast, in Figure 6a, the interfacial free energy of the PL phase relative to that of G decreases as f_A increases, driving the PL phase to become stable over the G phase at the vicinity of the lamellar phase region. In Figure 6c, the interfacial free energy of the PL phase becomes higher than that of G, leading to the vanishing of the stability region of PL.

The free energy comparison shown in Figure 6 shows that the PL phase is stabilized by its favorable interfacial free energy relative to the G phase. However, the free energy itself does not provide detailed information about the origin of this effect. We need to provide evidence to elucidate how the tethering position of the ABA_T optimizes the interfacial free energy while not increasing the entropic penalty of PL relative to G. In a previous work, we have demonstrated that local segregation of different block copolymers in an AB/AB diblock copolymer blend provides an important mechanism to stabilize intricate structures such as the complex spherical packing phases, or the Frank−Kasper phases, composed of minority polymeric domains of different sizes and shapes.[65] In particular, the local segregation of different block copolymers within each sphere-like domain leads to nonuniform distributions of the two copolymers at the nonspherical interface. Specifically, the symmetric/asymmetric copolymers are preferentially located on the interfacial areas of low/high curvatures. It is this nonuniform distribution of copolymers benefiting the formation of large polymeric domains and thus favoring the formation of minority domains of different sizes and shapes.

For the current case of ABA_T copolymers, we hypothesize that the local segregation of the different blocks might provide a mechanism to stabilize the simultaneous coexistence of flat lamellae and curved pores. Specifically, because of their different topological environments the two different (bridge and tail) B blocks may be locally segregated to accommodate to the two very different interfacial curvatures (i.e., layers and pores) existing in a PL morphology. In order to demonstrate this mechanism, the distributions of the B_1 and B_2 blocks for a typical set of parameters are plotted in Figure 7. From the SCFT results, it is obvious that the distributions of the two different B blocks are not uniform, indicating that local segregation of the bridge and tail B blocks does occur in the system. Furthermore, the B_1 blocks are concentrated at the A/B interfaces (Figure 7b), revealing that most of the B_1 blocks adopt a looping configuration because the B_1 block is too short to form a bridging configuration when τ = 0.25. This observation implies that the B_1-loops are arranged into a brush-like layer separating the A blocks and B_2 blocks. Accordingly, the curvature of the AB interface results in denser looping brushes inside the pores, thus lowering the concentration of the B_2 blocks there.

Normally, the formation of curved interfaces would lead to an increase of the interfacial area and thus the associated contribution to the interfacial free energy. Consequently, the size of the pore dictates how much B blocks could be embedded in the A layer and thus the associated contribution to the interfacial energy. The geometric size of the pores could be described by the diameter of the pore d_{pore} and the thickness of B layer l_B, which are shown as a function of τ at f_A = 0.21 in Figure 7c. It is interesting to note that d_{pore} varies non-monotonically as τ increases, *i.e.*, d_{pore} decreases to reach a minimum and then increases. When τ or f_{B_1} is very small, the total volume fraction B_1 blocks is much smaller than f_{B_2}. Accordingly, a significant portion of B_2 blocks has to enter the pores to expand the pores and thus to maintain the layered structure. In other words, the pore is significantly swollen by the long B_2 blocks. As τ increases, on one hand, the content of B_2 blocks in the pore is lowered. On the other hand, the swelling B_2 block is shortened. As a result, the pore shrinks as τ increases. As long as the pore is mainly filled by B_1 blocks, its size is mainly dictated by the length of B_1 block. Therefore, the pore size rises up after passing the minimal point. Obviously,

DOI: 10.1021/acs.macromol.7b02389
Macromolecules 2018, 51, 1529−1538

the variation trend of the thickness of B layer is opposite to that of the pore size.

The comparison of the interfacial and entropic contributions to the free energy between the PL and G phases shown in Figure 7d suggests that the favorable interfacial free energy of PL relative to G is closely related to the pore size coupled with the thickness of the B layer. The PL phase with smaller pores exhibits more favorable interfacial contribution. Although, at the same time, the entropic contribution becomes more unfavorable, the PL phase becomes more stable over the gyroid phase. From these observations, it could be concluded that the tethering position of the ABA_T copolymers provides a facile route to regulate the interfacial free energy of the PL phase at the low expense of entropic contribution relative to the gyroid phase, thus stabilizing the PL phase. Because of the favorable interfacial free energy, the PL phase is more likely to become stable over G at the stronger segregation region where the contribution of interfacial free energy becomes dominant, e.g., the PL phase completely replacing the G phase in Figure 1a with $\tau = 0.25$. In addition, it is also interesting to note that the lower mean curvature of PL than G enables the PL phase to have a lower interfacial free energy.[10]

In a brief, the critical factor of stabilizing the PL phase over the classical G phase arises from the local segregation between B_1 and B_2 blocks that occurs due to the formation of looping configurations of short B_1 blocks localized at the A/B interface by the topological constraint. As τ increases, increasing B_1 block has a higher probability to form bridging configurations instead of looping ones. The bridging configuration favors mixing B_1 blocks with B_2 blocks, thus lessening their local segregation. Without a high local segregation of B_1-/B_2 blocks, the PL phase loses its stability on the G phase. This is why the G phase reappears when $\tau > 0.29$ in Figure 4.

Why there is a large window of the hcp phase between the disordered phase and the cylinder phase in the parameter range of $0.30 < \tau < 0.42$ (Figure 4) is another fascinating question. Detailed free-energy comparison of the different ordered phases shown in Figure 5 confirms this observation. Note that the previous highly accurate SCFT results by Matsen indicated that the hcp phase is slightly more favorable than the face-centered-cubic (fcc) phase and their free energy difference is very tiny.[66] Thus, we only consider the hcp phase in this work. According to our previous work, one of the possible factors that may reverse the relative stability between hcp and bcc in the parameter region far from the order−disorder phase boundary is the adjustable bridge connecting neighboring spherical domains.[48,54] In multiarm AB-type block copolymers, the effect of combinatorial entropy of the multiple arms drives them to be partitioned into different neighboring domains as many as possible.[48] However, when the bridging blocks are shortened under the condition of fixed compositions, the proportion of the bridging configurations is lowered, which is accompanied by a loss of the combinatorial entropy. One simple way to reduce the stretching of the bridging blocks is to decrease the domain spacing while maintaining the crystalline arrangement. Because of the mass conservation, at the same time the domain size has to be reduced, resulting in an increase of interfacial free energy. Another useful way to release the stretching energy and at the same time to avoid disrupting the bridging configurations is to change the domain arrangement from the crystalline lattice of high coordination number (CN) to that of lower CN, which can beneficially reduce the domain spacing but not the domain size.

For the ABA_T copolymers, there should be a certain probability for the two A blocks belonging to the same polymer to be partitioned into two different A domains, especially for relatively large τ, thus enforcing the middle B_1 block to adopt bridging configurations. Moreover, the length of the bridging B_1 block is adjustable by τ. This hypothesis could be confirmed by an analysis of the SCFT results, which in turn rationalizes the transition between hcp and bcc in the large window of spherical phases with $0.375 < \tau < 0.5625$ via the concept of the adjustable bridges. It has been established that the crystalline phase of low CN is more likely to be formed as the bridging block is shortened.[18] Obviously, the decreasing length of the bridging B_1 block as τ decreases drives bcc to transform into hcp because hcp has lower CN than bcc,[18] which benefits delaying the disruption of the bridging configurations. An efficient algorithm for the calculation of the proportion of bridging configurations has been developed by Matsen and co-workers.[27,67] Figure 8 indicates that higher probability of bridging configurations is consistently achieved in hcp than in bcc.

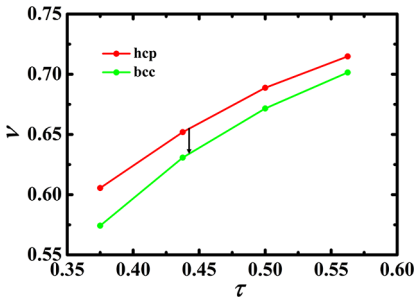

Figure 8. Comparison of the probability of bridging configurations between the hcp and bcc phases along the phase path of $f_A = 0.22$ for $^3/_8 \le \tau \le {}^9/_{16}$. The arrow indicates the hcp/bcc transition.

Additionally, a general phase sequence of L→ G → C→ bcc (or hcp) is observed for a fixed value of f_A from the phase diagram of Figure 4. This implies that the trend of segregation changes from strong to weak as τ increases. To confirm this observation quantitatively, we calculate the order−disorder transition $(\chi N)_{ODT}$ as a function of τ for various values of f_A = 0.2, 0.3, 0.4, and 0.5 (Figure 9). Interestingly, $(\chi N)_{ODT}$ increases to reach a maximum at around $\tau = 0.5$ and then decreases, indicating an opposite variation trend of the segregation degree. In the parameter space of Figure 4, the segregation degree declines as τ increases. Specifically, the A_2B

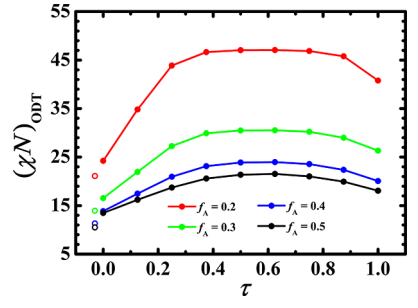

Figure 9. Order−disorder transition as a function of τ for f_A = 0.2, 0.3, 0.4, and 0.5, respectively. Four unfilled circles in red, green, blue, and black colors indicate $(\chi N)_{ODT} \approx 21.098$, 13.935, 11.324, and 10.495 of AB diblock copolymers for f_A = 0.2, 0.3, 0.4, and 0.5, respectively.

DOI: 10.1021/acs.macromol.7b02389
Macromolecules 2018, 51, 1529−1538

star copolymer at $\tau = 0$ has a stronger segregation than ABA triblock because joining the two A blocks together in A_2B benefits their separation from B blocks in contrast to the topological separation of the two A blocks in ABA.

The nonmonotonic change of ODT or the segregation degree is mainly governed by the separation between the divided B blocks and the tethered A block, while it is less influenced by the other A block linked at the end of B_1 block. In other words, the ODT of the AB-type copolymer composed of one B block tethered by an A block also varies nonmonotonically as the tethering position moves along the B block from one end to the other end. Obviously, the AB-type copolymer becomes AB diblock when the A block is linked at either of the two ends of the B block, while it becomes AB_2 miktoarm star copolymer. The results of ODT in Figure 9 suggest that the ODT of AB_2 (or A_2B) is consistently higher than that of AB with the same composition. In a brief, dividing the B block into two B_1- and B_2 blocks reduces the segregation degree between A and B blocks. As a result, as the tethering position of A block moves along the B block, the ODT increases to reach a maximum when the A block is tethered at the center of the B block and then it decreases. Considering the trivial effect of the connection of the another A block at the end of B_1 block, the ODT of ABA_T exhibits a nonmonotonic behavior with a maximum at around $\tau = 0.5$.

CONCLUSIONS

In summary, the self-assembly of ABA_T block copolymers has been systematically studied using the self-consistent field theory. Three phase diagrams of ABA_T with different tethering positions of the second A block are constructed. Surprisingly, a large window of the PL phase is identified in the f_A-χN phase diagram at certain tethering positions, *e.g.*, $\tau = 0.25$, which completely replaces the gyroid phase at relative strong segregation. The spatial distributions of the two B blocks divided by the tethering point reveals that the PL phase is stabilized by the local segregation between the two B blocks. The middle B_1 block and the tail B_2 block tend to accommodate to different interfacial curvatures due to their distinct topological environments and thus are preferentially located into the pores and the B layer of PL, respectively. As a result, the local segregation of the two B blocks in the PL phase leads to a favorable interfacial free energy at a reasonably low cost of entropic contribution to the free energy, and thus makes the PL phase become more stable over the gyroid phase. Therefore, the stabilization mechanism of complex ordered phases with highly nonuniform interfacial curvatures via the local segregation between two different blocks, originally proposed in the binary blend of AB/AB diblock copolymers,[65] is successfully generalized to the block copolymer melts. The robustness of this mechanism opens an avenue for the fabrication of nonclassical ordered phases. In addition, our results would renew the conventional understanding on the relative stability between the PL and G phases because it is tunable via designing the topology or architecture of AB-type block copolymers.

In addition, the observation of a large stability region of the hcp spherical phase in the phase diagram of Figure 4 with $0.30 < \tau < 0.42$ is also fascinating, which is 6−27 times wider than the ordinary channel of hcp in the phase diagrams of many known AB-type block copolymers including AB diblock, ABA triblock, AB_2 star, and ABABAB··· multiblock. Such large window of hcp must facilitate the observation of the hcp phase in experiments. Moreover, the direct transition from hcp to the cylinder phase is rather unusual. For advanced synthetic techniques, it is not difficult to make the ABA_T copolymers, and it is feasible to precisely control the tethering position of the additional A block, too. Therefore, these unusual self-assembly behaviors might be observed by experiment in the future.

AUTHOR INFORMATION

Corresponding Author

*(W.L.) E-mail: weihuali@fudan.edu.cn.

ORCID

Weihua Li: 0000-0002-5133-0267

An-Chang Shi: 0000-0003-1379-7162

Author Contributions

¶These authors contributed equally.

Notes

The authors declare no competing financial interest.

ACKNOWLEDGMENTS

This work was supported by National Natural Science Foundation of China (Grants Nos. 21574026 and 21774025) and the Natural Science and Engineering Research Council (NSERC) of Canada.

REFERENCES

(1) Bates, F. S.; Fredrickson, G. H. Block Copolymer Thermodynamics-Theory and Experiment. *Annu. Rev. Phys. Chem.* **1990**, *41*, 525−557.

(2) Darling, S. B. Directing the Self-assembly of Block Copolymers. *Prog. Polym. Sci.* **2007**, *32*, 1152−1204.

(3) Bates, F. S.; Hillmyer, M. A.; Lodge, T. P.; Bates, C. M.; Delaney, K. T.; Fredrickson, G. H. Multiblock polymers: Panacea or Pandora's Box? *Science* **2012**, *336*, 434−440.

(4) Li, W. H.; Müller, M. Defects in the Self-assembly of Block Copolymers and Their Relavance for Directed Self-assembly. *Annu. Rev. Chem. Biomol. Eng.* **2015**, *6*, 187−216.

(5) Förster, S.; Khandpur, A. K.; Zhao, J.; Bates, F. S.; Hamley, I. W.; Ryan, A. J.; Bras, W. Complex Phase Behavior of Polyisoprene-Polystyrene Diblock Copolymers Near the Order-Disorder Transition. *Macromolecules* **1994**, *27*, 6922−6935.

(6) Bates, F. S.; Fredrickson, G. H. Conformational Asymmetry and Polymer-Polymer Thermodynamics. *Macromolecules* **1994**, *27*, 1065−1067.

(7) Matsen, M. W.; Schick, M. Stable and Unstable Phases of a Diblock Copolymer Melt. *Phys. Rev. Lett.* **1994**, *72*, 2660−2663.

(8) Khandpur, A. K.; Förster, S.; Bates, F. S.; Hamley, I. W.; Ryan, A. J.; Bras, W.; Almdal, K.; Mortensen, K. Polyisoprene-Polystyrene Diblock Copolymer Phase Diagram near the Order-Disorder Transition. *Macromolecules* **1995**, *28*, 8796−8806.

(9) Bates, F. S.; Fredrickson, G. H. Block Copolymers-Designer Soft Material. *Phys. Today* **1999**, *52*, 32−38.

(10) Matsen, M. W. The Standard Gausian Model for Block Copolymer Melts. *J. Phys.: Condens. Matter* **2002**, *14*, R21−R47.

(11) Tyler, C. A.; Morse, D. C. Orthorhombic Fddd Network in Triblock and Diblock Copolymer Melts. *Phys. Rev. Lett.* **2005**, *94*, 208302.

(12) Cochran, E. W.; Garcia-Cervera, C. J.; Fredrickson, G. H. Stability of the Gyroid Phase in Diblock Copolymers at Strong Segregation. *Macromolecules* **2006**, *39*, 2449−2451.

(13) Hajduk, D. A.; Harper, P. E.; Gruner, S. M.; Honeker, C. C.; Kim, G.; Thomas, E. L.; Fetters, L. J. The Gyroid: A New Equilibrium Morphology in Weakly Segregated Diblock Copolymers. *Macromolecules* **1994**, *27*, 4063−4075.

DOI: 10.1021/acs.macromol.7b02389
Macromolecules 2018, 51, 1529−1538

(14) Matsen, M. W. Effect of Architecture on the Phase Behavior of AB-type Block Copolymer Melts. *Macromolecules* **2012**, *45*, 2161−2165.
(15) Lee, S.; Bluemle, M. J.; Bates, F. S. Discovery of a Frank-Kasper σ Phase in Sphere-Forming Block Copolymer Melts. *Science* **2010**, *330*, 349−353.
(16) Lee, S. W.; Leighton, C.; Bates, F. S. Sphericity and Symmetry Breaking in the Formation of Frank-Kasper phases from One Component Materials. *Proc. Natl. Acad. Sci. U. S. A.* **2014**, *111*, 17723−17731.
(17) Kim, K.; Schulze, M. W.; Arora, A.; Lewis, R. M.; Hillmyer, M. A.; Dorfman, K. D.; Bates, F. S. Thermal Processing of Diblock Copolymer Melts Mimics Metallurgy. *Science* **2017**, *356*, 520−523.
(18) Xie, N.; Li, W. H.; Qiu, F.; Shi, A.-C. σ Phase Formed in Conformationally Asymmetric AB-type Block copolymers. *ACS Macro Lett.* **2014**, *3*, 906−910.
(19) Li, W. H.; Duan, C.; Shi, A.-C. Non-Classical Spherical Packing Phases Self-Assembled From AB-Type Block Copolymers. *ACS Macro Lett.* **2017**, *6*, 1257−1262.
(20) Geiser, D.; Höcker, H. Synthesis and Investigation of Macrocyclic Polystyrene. *Macromolecules* **1980**, *13*, 653−656.
(21) Hadjichristidis, N.; Pitsikalis, M.; Pispas, S.; Iatrou, H. Polymers with Complex Architecture by Living Anionic Polymerization. *Chem. Rev.* **2001**, *101*, 3747−3792.
(22) Nagata, Y.; Masuda, J.; Noro, A.; Cho, D.; Takano, A.; Matsushita, Y. Preparation and Characterization of a Styrene-Isoprene Undecablock Copolymer and Its Hierarchical Microdomain Structure in Bulk. *Macromolecules* **2005**, *38*, 10220−10225.
(23) Matsumiya, Y.; Watanabe, H.; Takano, A.; Takahashi, Y. Uniaxial Extensional Behavior of $(SIS)_p$-Type Multiblock Copolymer Systems: Structural Origin of High Extensibility. *Macromolecules* **2013**, *46*, 2681−2695.
(24) Pang, X. C.; Zhao, L.; Akinc, M.; Kim, J. K.; Lin, Z. Q. Novel Amphiphilic Multi-Arm, Star-Like Block Copolymers as Unimolecular Micelles. *Macromolecules* **2011**, *44*, 3746−3752.
(25) Zhang, J. Y.; Li, T. Q.; Mannion, A. M.; Schneiderman, D. K.; Hillmyer, M. A.; Bates, F. S. Tough and Sustainable Graft Block Copolymer Thermoplastics. *ACS Macro Lett.* **2016**, *5*, 407−412.
(26) Bates, C. M.; Bates, F. S. 50th Anniversary Perspective: Block Polymers Pure Potential. *Macromolecules* **2017**, *50*, 3−22.
(27) Matsen, M. W.; Thompson, R. B. Equilibrium Behavior of Symmetric ABA Triblock Copolymer Melts. *J. Chem. Phys.* **1999**, *111*, 7139−7146.
(28) Matsen, M. W. Equilibrium Behavior of Asymmetric ABA Triblock Copolymer Melts. *J. Chem. Phys.* **2000**, *113*, 5539−5544.
(29) Mai, S.-M.; Mingvanish, W.; Turner, S. C.; Chaibundit, C.; Fairclough, J. P. A.; Heatley, F.; Matsen, M. W.; Ryan, A. J.; Booth, C. Microphase-Separation Behavior of Triblock Copolymer Melts. Comparison with Diblock Copolymer Melts. *Macromolecules* **2000**, *33*, 5124−5130.
(30) Hamersky, M. W.; Smith, S. D.; Gozen, A. O.; Spontak, R. J. Phase Behavior of Triblock Copolymers Varying in Molecular Asymmetry. *Phys. Rev. Lett.* **2005**, *95*, 168306.
(31) Li, W.; Delaney, K. T.; Fredrickson, G. H. Fddd Network Phase in ABA Triblock Copolymer Melts. *J. Polym. Sci., Part B: Polym. Phys.* **2016**, *54*, 1112−1117.
(32) Sakurai, S.; Shirouchi, K.; Munakata, S.; Kurimura, H.; Suzuki, S.; Watanabe, J.; Oda, T.; Shimizu, N.; Tanida, K.; Yamamoto, K. Morphology Reentry with a Change in Degree of Chain Asymmetry in Neat Asymmetric Linear A_1BA_2 Triblock Copolymers. *Macromolecules* **2017**, *50*, 8647−8657.
(33) Hadjichristidis, N.; Iatrou, H.; Behal, S. K.; Chludzinski, J. J.; Disko, M. M.; Garner, R. T.; Liang, K. S.; Lohse, D. J.; Milner, S. T. Morphology and Miscibility of Miktoarm Styrene-Diene Copolymers and Terpolymer. *Macromolecules* **1993**, *26*, 5812−5815.
(34) Yang, L. Z.; Hong, S.; Gido, S. P.; Velis, G.; Hadjichristidis, N. I_5S Miktoarm Star Block Copolymers: Packing Constraints on Morphology and Discontinuous Chevron Tilt Grain Boundaries. *Macromolecules* **2001**, *34*, 9069−9073.
(35) Grason, G. M.; Kamien, R. D. Interfaces in Diblocks: A Study of Miktoarm Star Copolymers. *Macromolecules* **2004**, *37*, 7371−7380.
(36) Shi, W. C.; Tateishi, Y. C.; Li, W.; Hawker, C. J.; Fredrickson, G. H.; Kramer, E. J. Producing Small Domain Features Using Miktoarm Block Copolymers with Large Interaction Parameters. *ACS Macro Lett.* **2015**, *4*, 1287−1292.
(37) Matsen, M. W.; Schick, M. Microphase Separation in Starblock Copolymer Melts. *Macromolecules* **1994**, *27*, 6761−6767.
(38) Xu, Y. C.; Li, W. H.; Qiu, F.; Lin, Z. Q. Self-assembly of 21-arm Star-like Diblock Copolymer in Bulk and Under Cylindrical Confinement. *Nanoscale* **2014**, *6*, 6844−6852.
(39) Burns, A. B.; Register, R. A. Mechanical Properties of Star Block Polymer Thermoplastic Elastomers with Glassy and Crystalline End Blocks. *Macromolecules* **2016**, *49*, 9521−9530.
(40) Zhang, L. S.; Lin, J. P.; Lin, S. L. Effect of Molecular Architecture on Phase Behavior of Graft Copolymers. *J. Phys. Chem. B* **2008**, *112*, 9720−9728.
(41) Wang, L. Q.; Zhang, L. S.; Lin, J. P. Microphase Separation in Multigraft Copolymer Melts Studied by Random-phase Approximation and Self-consistent Field Theory. *J. Chem. Phys.* **2008**, *129*, 114905.
(42) Matsen, M. W.; Schick, M. Stable and Unstable Phases of a Linear Multiblock Copolymer Melt. *Macromolecules* **1994**, *27*, 7157−7163.
(43) Spontak, R. J.; Smith, S. D. Perfectly-Alternating Linear $(AB)_n$ Multiblock Copolymers: Effect of Molecular Design on Morphology and Properties. *J. Polym. Sci., Part B: Polym. Phys.* **2001**, *39*, 947−955.
(44) Rasmussen, K. Ø.; Kober, E. M.; Lookman, T.; Saxena, A. Morphology and Bridging Properties of $(AB)_n$ Multiblock Copolymers. *J. Polym. Sci., Part B: Polym. Phys.* **2003**, *41*, 104−111.
(45) Nap, R.; Sushko, N.; Erukhimovich, I.; ten Brinke, G. Double Periodic Lamellar-in-Lamellar Structure in Multiblock Copolymer Melts with Competing Length Scales. *Macromolecules* **2006**, *39*, 6765−6770.
(46) Zhao, B.; Jiang, W. B.; Chen, L.; Li, W. H.; Qiu, F.; Shi, A.-C. Emergence and Stability of a Hybrid Lamella?Sphere Structure from Linear ABAB Tetrablock Copolymers. *ACS Macro Lett.* **2018**, *7*, 95−99.
(47) Lynd, N. A.; Oyerokun, F. T.; O'Donoghue, D. L.; Handlin, D. L., Jr.; Fredrickson, G. H. Design of Soft and Strong Thermoplastic Elastomers Based on Nonlinear Block Copolymer Architectures Using Self-Consistent-Field Theory. *Macromolecules* **2010**, *43*, 3479−3486.
(48) Gao, Y.; Deng, H. L.; Li, W. H.; Qiu, F.; Shi, A.-C. Formation of Nonclassical Ordered Phases of AB-type Multi-arm Block Copolymers. *Phys. Rev. Lett.* **2016**, *116*, 068304.
(49) Lee, W. B.; Elliott, R.; Mezzenga, R.; Fredrickson, G. H. Novel Phase Morphologies in a Microphase-Separated Dendritic Polymer Melt. *Macromolecules* **2009**, *42*, 849−859.
(50) Jiang, W. B.; Qiang, Y. C.; Liu, M. J.; Li, W. H.; Qiu, F.; Shi, A.-C. Tetragonal Phase of Cylinders Self-assembled from Binary Blends of AB Diblock and $(A'B)_n$ Star Copolymers. *Phys. Chem. Chem. Phys.* **2017**, *19*, 25754−25763.
(51) Matsen, M. W. Phase Behavior of Block Copolymer/Homopolymer Blends. *Macromolecules* **1995**, *28*, 5765−5773.
(52) Matsen, M. W. Stabilizing New Morphologies by Blending Homopolymer with Block Copolymer. *Phys. Rev. Lett.* **1995**, *74*, 4225.
(53) Arora, A.; Qin, J.; Morse, D. C.; Delaney, K. T.; Fredrickson, G. H.; Bates, F. S.; Dorfman, K. D. Broadly Accessible Self-Consistent Field Theory for Block Polymer Materials Discovery. *Macromolecules* **2016**, *49*, 4675−4690.
(54) Xie, N.; Liu, M. J.; Deng, H. L.; Li, W. H.; Qiu, F.; Shi, A.-C. Macromolecular Metallurgy of Binary Mesocrystals via Designed Multiblock Terpolymers. *J. Am. Chem. Soc.* **2014**, *136*, 2974−2977.
(55) Liu, M. J.; Li, W. H.; Qiu, F.; Shi, A.-C. Stability of σ phase in B_1AB_2C tetrablock terpolymers. *Soft Matter* **2016**, *12*, 6412−6421.
(56) Grason, G. M.; DiDonna, B. A.; Kamien, R. D. Geometric Theory of Diblock Copolymer Phases. *Phys. Rev. Lett.* **2003**, *91*, 058304.

DOI: 10.1021/acs.macromol.7b02389
Macromolecules 2018, 51, 1529−1538

(57) Grason, G. M.; Kamien, R. D. Self-consistent Field Theory of Multiply Branched Block Copolymer melts. *Phys. Rev. E* **2005**, *71*, 051801.
(58) Shi, A.-C. *Developments in Block Copolymer Science and Technology*; John Wiley & Sons, Ltd.: New York, 2004.
(59) Fredrickson, G. H. *The Equilibrium Theory of Inhomogeneous Polymers*; Oxford University Press: New York, 2006.
(60) Rasmussen, K. Ø.; Kalosakas, G. Improved Numerical Algorithm for Exploring Block Copolymer Mesophases. *J. Polym. Sci., Part B: Polym. Phys.* **2002**, *40*, 1777−1783.
(61) Tzeremes, G.; Rasmussen, K. Ø.; Lookman, T.; Saxena, A. Efficient Computation of The Structural Phase Behavior of Block Copolymers. *Phys. Rev. E: Stat. Phys., Plasmas, Fluids, Relat. Interdiscip. Top.* **2002**, *65*, 041806.
(62) Thompson, R. B.; Rasmussen, K. Ø.; Lookman, T. Improved Convergence in Block Copolymer Self-consistent Field Theory by Anderson Mixing. *J. Chem. Phys.* **2004**, *120*, 31−34.
(63) Li, W. H.; Shi, A.-C. *Self-assemblying Systems Theory and Simulation*; John Wiley & Sons, Ltd.: New York, 2017; pp 85−107.
(64) Xu, Y. C.; Li, W. H.; Qiu, F.; Zhang, H. D.; Yang, Y. L.; Shi, A.-C. Stability of Hierarchical Lamellar Morphologies Formed in ABC Star Triblock Copolymers. *J. Polym. Sci., Part B: Polym. Phys.* **2010**, *48*, 1101−1109.
(65) Liu, M. J.; Qiang, Y. C.; Li, W. H.; Qiu, F.; Shi, A.-C. Stabilizing the Frank-Kasper Phases via Binary Blends of AB Diblock Copolymers. *ACS Macro Lett.* **2016**, *5*, 1167−1171.
(66) Matsen, M. W. Fast and Accurate SCFT Calculations for Periodic Block-Copolymer Morphologies Using the Spectral Method with Anderson Mixing. *Eur. Phys. J. E: Soft Matter Biol. Phys.* **2009**, *30*, 361−369.
(67) Spencer, R. K. W.; Matsen, M. W. Domain Bridging in Thermoplastic Elastomers of Star Block Copolymer. *Macromolecules* **2017**, *50*, 1681−1687.

DOI: 10.1021/acs.macromol.7b02389
Macromolecules 2018, 51, 1529−1538